Multi-frequency Power Angular Spectrum Comparison for an Indoor Environment

Usman Tahir Virk*, Sinh. L. H. Nguyen*, Katsuyuki Haneda*
*Department of Radio Science and Engineering, Aalto University, Espoo, Finland.
Email: usman.virk@aalto.fi

***Abstract*—This paper presents the comparison of power angular spectra at frequencies below and above 6 GHz, i.e., 2, 15, 28, 60 GHz. With the increased focus on millimeter wave frequencies for ultra-high data rates, a detailed understanding of channel frequency dependence has become crucial. The analysis in this paper is based on multi-frequency radio channel measurements in an indoor coffee room environment for both line-of-sight (LOS) and non-LOS (NLOS) scenarios. For multipath extraction, two different methodologies are used at below and above 6 GHz frequency bands, respectively. The results indicate that LOS channels demonstrate a similar spatial spread at all the frequencies considered, and hence can be spatially modeled in a similar fashion. The NLOS channels exhibit larger spatial spread overall. The paths at above 6 GHz channels appear to be spatially more consistent compared to those that are below 6 GHz, where penetrated and diffracted paths also exist.**

***Index Terms*—frequency dependence, power angular spectrum, radio channel measurements.**

I. Introduction

The accelerated demand for higher data rates has attracted a significant amount of research in millimeter wave frequency bands for future wireless systems. This due to highly underutilized frequency spectrum in these bands. Therefore, the quest for innovative solutions enabling 5G and beyond has driven huge investments by the stakeholders world wide.

Serious efforts have been devoted for the standardization of 5G specifications at the standard bodies such as International Telecommunication Union (ITU) and Third Generation Partnership project (3GPP). This highly encourages the scientific research dealing with different aspects of the radio channel modeling. A high degree of expectation is associated with 5G wireless networks for the provision of at least 1 Gbps data rate for all users as a uniform user data rate experience, and as rich as 5 to 50 Gbps data rate for mobile users [1], [2].

Frequency dependency and spatial distribution of multipaths in different radio channels are some of the critical aspects of radio channel modeling that require thorough investigations, and are important from system design and performance analysis perspective [3]. A careful literature survey reveals limited studies where radio channels are compared at a wide range of frequency bands for evaluating a frequency dependent behavior, especially below and above 6 GHz. A comparative analysis of power, delay and angular characteristics for cm- and mm-wave frequencies are reported in [4]-[11] and references therein. However, the measurements involved in these studies are performed in diverse conditions making the comparability of channels equivocal. The studies in [12]-[14] provide comparison of power delay profiles between 3 and 60 GHz frequency bands based on simultaneous channel sounding for cellular and WiFi scenarios but lack directional characteristics.

The goal of this paper is to investigate the frequency dependency of radio channels and multipath spatial consistency in these channels by analyzing the power angular spectrum (PAS), angular distribution of paths, and path angular profile (PAP) at frequencies below and above 6 GHz. The analysis is based on measurements that were conducted in a consistent manner to ensure reasonable degree of comparability.

The paper is organized in four sections. Section II presents extensive multi-frequency radio channel measurements with details on the channel sounders and the measurement campaigns. Section III introduces the multipath extraction methodologies. For discernment, PAS results are discussed with different graphical interpretations in the Results and Discussions, Section IV. Finally conclusions are drawn based on the analysis in the preceding section.

II. Multi-frequency Radio Channel Sounding

A. Channel sounders

A vector network analyzer (VNA) based channel sounder is employed for channel measurements at the desired radio frequency (RF) bands, i.e., 2, 15, 28 and 60 GHz. In the channel sounder, VNA is the core data acquisition component that allows delay- and phase-synchronized measurements. The same RF bandwidth of 3 GHz for all frequency bands leads to a high delay resolution of $1/3$ ns. For each frequency band, slight modifications are made in the channel sounder setup to achieve the channel sounding at that particular frequency band. Since the aim is to perform directional channel measurements to exploit the spatial characteristics of the radio channels, two different directional measurement setups are utilized for below and above 6 GHz frequency bands. For the below 6 GHz frequency band, a synthetic planar array of aperture size 30 cm is created by spatially scanning a single omni-directional bicone antenna element using an electro-mechanical positioner on the Rx side as illustrated through Fig. 1. At 30 cm array aperture size, the achievable angular resolution at the center frequency for below 6 GHz frequency band is 45°. The synthetic planar array consists of (12×12) antenna locations on an xy grid of the horizontal plane with neighboring two antenna locations separated by $\lambda/2$ at 6 GHz RF. However at

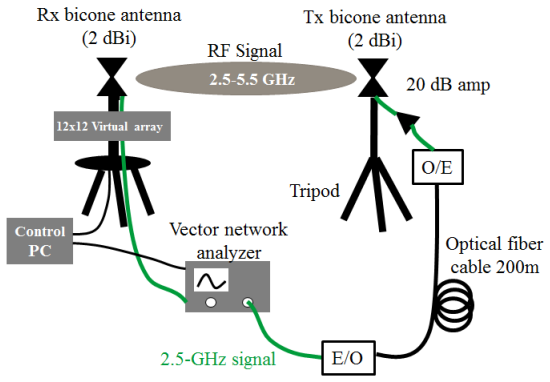

Fig. 1: Below 6 GHz channel sounder setup.

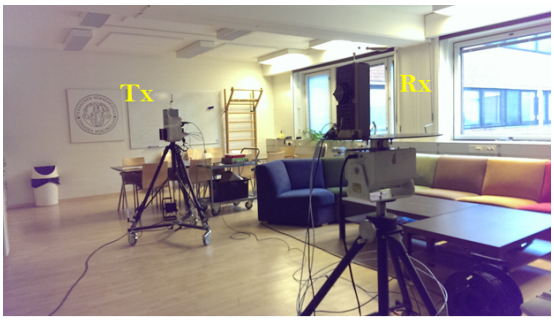

Fig. 2: A coffee room where the multi-frequency channel sounding took place.

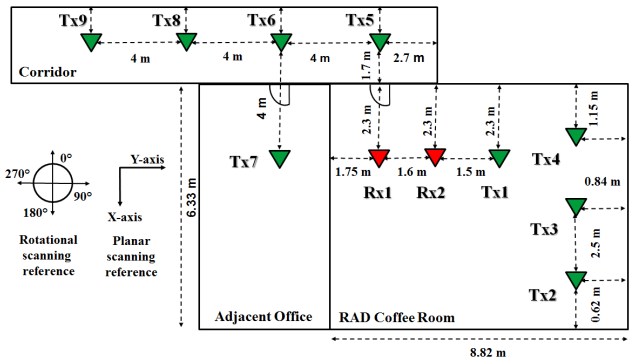

Fig. 3: Multi-frequency radio channel sounding environment layout.

the frequency bands above 6 GHz, rotational measurements are realized through an electro-mechanical rotator at the Rx side with a high gain horn antenna, as depicted in [8]. The horn antenna was rotated over the azimuth angles with a step size of 5° through a complete 360°; the elevation angle was set to 0°, i.e., the horizontal scan only. The horn antennas with same half-power beamwidth (HPBW) are used at 15, 28 and 60 GHz measurements for a consistent comparison of the spatial multipath channels.

In order to extend the frequency range of the VNA, channel measurements at 28 and 60 GHz are performed by mixing the VNA signals with local oscillator (LO) signals using frequency up- and down-converters, as illustrated and described comprehensively in [8], while there are no converters required at 2 and 15 GHz bands. The converters are harmonic mixers with internal frequency doublers. The channel sounders provide relatively different dynamic ranges depending on the RF. However, this has a negligible influence on the analysis since the noise floor drops from -120 dB to -145 dB for the lowest to the highest frequency band, respectively. Parameter settings of the channel sounder for respective frequencies along with the details on Tx and Rx antennas are summarized in Table I. The distance coverage of the sounder is extended by the use of an optical fiber cable between Tx and VNA transmit port.

B. Measurement Campaigns

The measurement campaigns at $2, 15, 28$ and 60 GHz frequency bands were performed in a coffee room, its adjacent corridor and an office room in Aalto University, Finland. The environment is depicted in Fig. 2. Both line-of-sight (LOS) and non-LOS (NLOS) scenarios were considered. In both of these scenarios, Rx locations were inside the coffee room while Tx was moved in and out of it depending on the scenario under consideration. The layout of the environment with all the measured locations is illustrated through Fig. 3. With two (02) Rx locations inside the coffee room, total nine (09) Tx locations were measured giving a total of (18) Tx-Rx links. Most of the Tx locations in the NLOS scenario were in the corridor adjacent to the coffee room. However, one NLOS Tx location was also measured in the adjacent office room. In order to maintain comparability of measurements at different frequency bands, the Tx and Rx locations were carefully marked, interior settings of the environment were retained, and measurements were carried out during weekends to avoid human interruption.

III. Multipath Extraction for Radio Channels

A. Below 6 GHz Frequency Band

The VNA acquires the channel transfer function $\mathrm{H}(m, f_i)$ for a particular Tx location, where $m \in 1, 2, ..., M = 144$ represent indices of antenna element position in the Rx synthetic planar array and f_i corresponds to RF at the i-th frequency bin, $i \in 1, 2, ..., I = 3001$.

For the AoA estimation at the Rx, a spatio-temporal beamforming is carried out for the propagation paths in the frequency domain. The beamformed channel over the given frequency tone, f_i, is given as

$$H_{\mathrm{BF}}(f_i, \phi) = \frac{\boldsymbol{w}^H(\phi)\mathrm{vec}\{\mathbf{H}(f_i)\}}{\|\boldsymbol{w}(\phi)\|_F}, \quad (1)$$

where $(\cdot)^H$ represents the conjugate transpose, the vector operator $\mathrm{vec}\{\cdot\}$ stacks the columns of its matrix argument on top of each other; $\boldsymbol{w}(\phi)$ is the beamforming weight vector; and $\|\cdot\|_F$ is the Frobenius norm. The beamforming weight vector at Rx, $\boldsymbol{w}(\phi)$, is equivalent to an array steering vector of a multipath component with the azimuth angle ϕ, as described in [15].

The strong paths, arriving at the Rx, are filtered from the power delay profile (PDP) using their propagation delay τ_n,

TABLE I: Summary of the channel sounder setup.

Description	2 GHz	15 GHz	28 GHz	60 GHz
Directional measurement	SIMO	Rotational		
Rx configuration	2D virtual array (12×12)	Rotational ($0° : 5° : 360°$)		
RF signal	2.5–5.5 GHz	13.5–16.5 GHz	27–30 GHz	61.5–64.5 GHz
Signal bandwidth	3 GHz			
Sweep points	3001	3001	2001	7501
IF signal	n/a	n/a	1–4 GHz	2.7–5.7 GHz
LO signal	n/a	n/a	13.5 GHz	14.5 GHz
Transmit power (VNA)	-15 dBm	-15 dBm	-20 dBm	-10 dBm
Tx Antenna	bicone (2 dBi), HPBW: $60°$ (elevation), omni-directional (azimuth)			
Rx Antenna	Same as Tx antenna	horn (19 dBi), HPBW: $40°$ (elevation), $10°$ (azimuth)		
Antennas polarization	vertical			
Antennas height	1.9 m			1.65 m
System calibration	back-to-back calibration with a 20-dB attenuator			

$1 \leq n \leq N_l$, N_l is the number of strong paths of the l-th link, $1 \leq l \leq 18$ in the present measurements. Finally, the wideband AoA estimates at the Rx, ϕ_n are obtained using the delay-filtered channels as

$$\phi_n = \arg\max_{\phi} \left| \sum_{i=1}^{I} \frac{\boldsymbol{w}^H(\phi)\text{vec}\{\mathbf{H}(f_i)\}}{\|\boldsymbol{w}(\phi)\|_F} \exp(-\text{j}2\pi f_i \tau_n) \right|. \tag{2}$$

For the below 6 GHz measurements, the wideband frequency covers the measurement bandwidth of 3 GHz. The path amplitudes is also estimated from (2) as the maximized cost function given by ϕ_n. We then compensate for a broadside gain of the Rx antenna to obtain the propagation path gain. For this approach, the spatial discrimination of paths depends on the antenna array aperture size, and improves as the aperture size increases.

B. Above 6 GHz Frequency Bands

In contrast to the multipath estimation based on beamforming method for below 6 GHz RF, a multi-dimensional multipath estimation for 15, 28 and 60 GHz measurements is carried out based on the local maxima search in the power-angular delay profile (PADP) obtained from the direction-scanning measurements at each of these frequency bands. For each band and Tx-Rx link, a PADP is calculated by taking the inverse Fourier transform of the measured channel transfer function $H(\phi, f_i)$ over the angular scanning range of $(\phi = 0°, 5°, 10°, ..., 360°)$, as presented in [8]. Thanks to the high time and spatial resolution of $1/3$ ns and $5°$ in the measurements, respectively, the two-dimensional search in delay and angle for the local maxima above the noise level in the PADP provides a coarse estimation of the power, delay and AoA of the detected paths [9]. In a single angular bin, only strong paths are detected over the delay by finding the peaks' amplitude above the local mean over a sliding delay window with an noise-eliminating threshold P_{th}. For the analysis in this paper, window size of 1.67 ns, and $P_{\text{th}} = 5$ dB are used to detect significant peaks while minimizing erroneous detection of noisy peaks. Finally, the angle and the power of each path is refined by matching the main beam pattern of the horn antenna with observed powers of the path at $(\phi_n - 5°), \phi_n$ and $(\phi_n + 5°)$ of the horn antenna orientation. This improves the azimuth angular estimates with an accuracy of $0.5°$. With the available horn antenna radiation patterns, the antenna gain was then compensated to obtain the respective path gain estimate. For further details on this method, the readers are referred to [8], [9] and the references therein. The set of the detected paths of l-th link is denoted by

$$P_l = \{P_n, \tau_n, \phi_n\}_{n=1}^{N_l}, \tag{3}$$

where P_n, τ_n, ϕ_n are the power, delay, and AoA of the n-th path with total N_l number of paths in the l-th link.

IV. Results and Discussions

A. Power Angular Spectrum

The power angular spectrum (PAS) of a channel is the marginal integral of the PADP over the delay domain. In order to filter out noise, the PADP was reproduced by convolving the extracted paths described in the Section III with the antenna gain patterns; the array patterns are used for the below 6 GHz, while the beam pattern of the horn antenna was used for above 6 GHz cases. The mathematical details on evaluating PAS are available in [8]. For the demonstration purpose, normalized PAS at all the frequencies under consideration are simultaneously plotted in the Fig. 4 (a-c) for the LOS links Tx1Rx1 and Tx3Rx1, and the NLOS link Tx6Rx1. In the LOS case, it is observed from Fig. 4(a-b) that below 6 GHz channel is richer in multipath compared to the channels at other frequencies. However, it can be seen that the strong paths spatially exist at all frequencies. Furthermore, good agreement of PAS can be seen at 15 and 28 GHz, similar to what is reported in [10]. It is also interesting to note that some paths

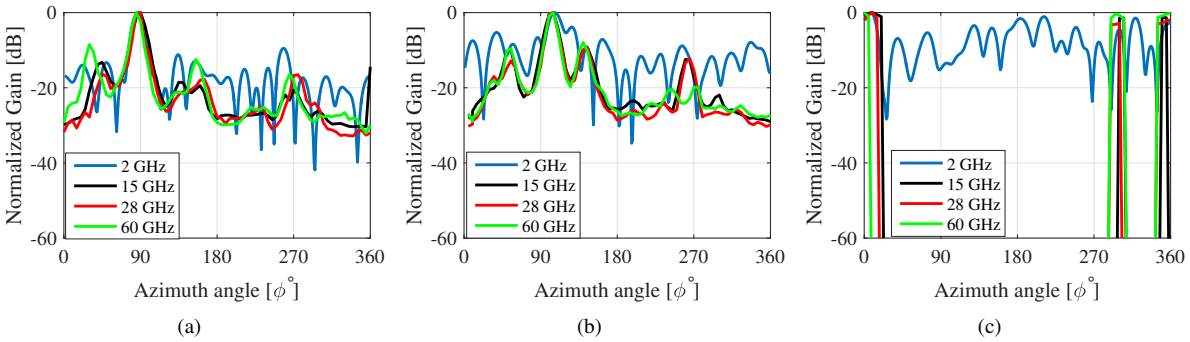

Fig. 4: Power angular spectrum (PAS) for (a) Tx1Rx1, (b) Tx3Rx1 and (c) Tx6Rx1 links; (a) and (b) are LOS channels while (c) is an NLOS link.

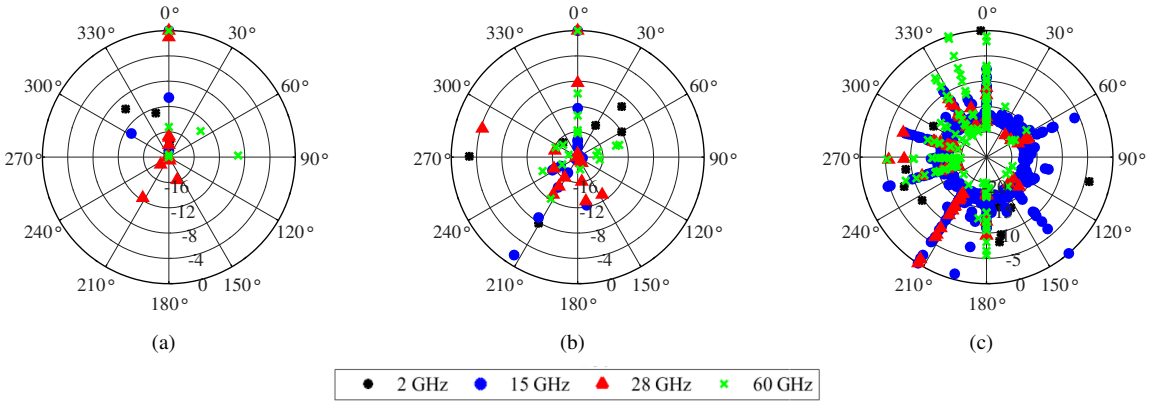

Fig. 5: Angular distributions of paths for (a) Tx1Rx1, (b) Tx3Rx1 and (c) Tx6Rx1 links; (a) and (b) are LOS channels while (c) is an NLOS link.

appear to be stronger in the normalized PAS at 60 GHz for the link Tx1Rx1 compared to the close contenders at 15 and 28 GHz, as seen in Fig. 4(b). For the NLOS case shown in Fig. 4(c), only few paths exist above 6 GHz frequencies and the PAS curves contain peaks at certain angles only. This is most likely due to higher attenuation in diffraction around wall corners and penetration through windows at above 6 GHz frequencies.

B. Angular Distributions of Paths

The extracted multipaths for the give radio channels are plotted in the polar format in Fig. 5(a-c) for the LOS links Tx1Rx1, Tx3Rx1 and the NLOS link Tx6Rx1. This allows us to observe the distribution of paths at the links from the channels at different frequencies. The circular and radial axes represent the angles and power levels of the multipaths, respectively. The path angles are normalized such that zero azimuth angle corresponds to the direction of Tx seen from the Rx, which refers to the LOS path in the LOS cases and a hypothetical wall penetrated paths in the NLOS cases. The paths power is normalized to the power of the strongest path. For convenience in visualizing, only 20 dB path dynamic range is considered in the plots. The weak paths are concentrated towards the center of the polar plots, while strong paths can be seen towards the circumference. With the 20 dB path dynamic range, more paths are observed in the NLOS case. From Fig. 5, it is worthwhile to point out a relatively better consistency in AoA of the paths for frequencies above 6 GHz. Due to low angular resolution below 6 GHz frequency band, a smaller number of paths can be seen at this band, making the comparison challenging for below and above 6 GHz frequency bands. However, some paths arrive at the Rx from relatively different directions in the considered frequency bands, which is more profound for the LOS case. Another noticeable fact is that the path distribution over the angles is almost identical in the LOS case for all frequencies; whereas it only appears to be more consistent for the frequencies above 6 GHz in case of NLOS. The slightly lower antenna heights in 60 GHz measurements, as indicated in Table I may be attributed to some of the noted differences compared to other frequency bands.

C. Power Angular Profile

In order to strengthen the analysis further, power angular profiles (PAPs) are presented in Fig. 6 for the LOS and Fig. 7 for the NLOS cases. The PAPs are derived by summing up paths from all the links at each RF within the angular bin width of 20°. The path angle and power normalization is carried out in a similar way as described in the previous Subsection IV-B. The figures overlay curves fitted with Gaussian distribution. For the LOS case, the standard deviation of the fitted Gaussian curve, σ_ϕ, is almost similar across the frequencies with a difference of only a few degrees. This essentially indicates that the LOS component is dominant, and hence the channels

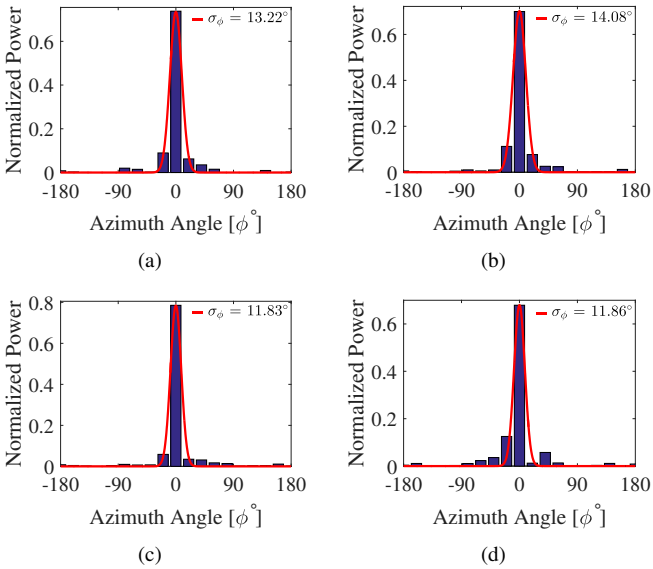

Fig. 6: PAPs of LOS links at (a) 2, (b) 15, (c) 28 and (d) 60 GHz. Their Gaussian fits are overlaid.

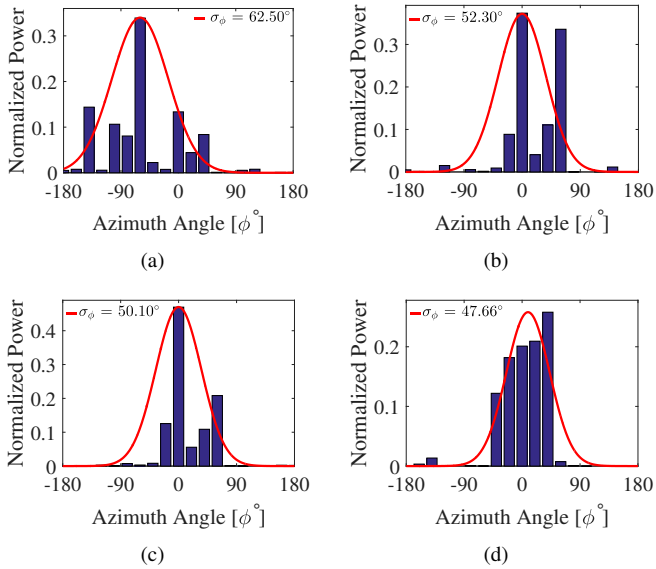

Fig. 7: PAPs of NLOS links at (a) 2, (b) 15, (c) 28 and (d) 60 GHz. Their Gaussian fits are overlaid.

can be spatially modeled in the same fashion at all frequencies. In the NLOS case, all channels exhibit larger spatial spread with the largest spread for below 6 GHz channels among all. This can be explained by the fact that some paths arrive at the Rx at below 6 GHz due to penetration through windows and walls, and diffraction around wall corners; those paths have too weak signal contribution at above 6 GHz.

V. Summary and Conclusions

The comparison of PAS, multipath angular distributions and PAP based on multi-frequency radio channel measurements in an indoor office environment is presented. Multipath extraction methods for below and above 6 GHz bands are described. Frequency dependency and the spatial consistency, or equivalently the angular selectivity, of the multipaths in different radio channels is investigated. The results demonstrate strong similarities in the spatial spread of the radio channels with LOS path domination, which allows them to be treated in a similar fashion from channel spatial modeling perspective. On the contrary, for the considered NLOS scenario, all channels exhibit large spatial spread, with below 6 GHz band offering the largest spread among all. The paths at above 6 GHz channels appear to be spatially more consistent compared to those that are below 6 GHz where penetrated and diffracted paths also exist.

Acknowledgment

The authors would like to thank the financial support of the Academy of Finland through the WiFiUS project Device-to-Device Communications at Millimeter-Wave Frequencies, decision number 284709. The authors also appreciate the assistance of Dr. Jan Jarvelainen, Mr. Sathya Narayana Venkatasubrimanyan, Mr. Adrian de Miguel, Mr. Muhammad Ali, and Mr. Reza Naderpour in the measurement campaigns.

References

[1] Samsung, "Technologies for Rel-12 and Onwards," *3GPP Workshop*, RWS-120021, June 2012.

[2] Z. Pi and F. Khan, "An Introduction to millimeter-wave mobile broadband systems," *IEEE Commun. Mag.*, vol. 49, no. 6, June 2011, pp. 10107.

[3] J. Medbo *et al.*, "Channel modelling for the fifth generation mobile communications," in *Proc. 8th Eur. Conf. on Antennas and Propag. (EuCAP'14)*, The Hague, Apr. 2014, pp. 219–223.

[4] G. Maccartney *et al.*, "Indoor office wideband millimeter-wave propagation measurements and channel models at 28 and 73 GHz for ultra-dense 5G wireless networks," *IEEE Access*, vol. 3, pp. 2388–2424, 2015.

[5] J. Medbo, N. Sei, and H. Asplund, "Frequency dependency of measured highly resolved directional propagation channel characteristics," in *Proc. 22th Eur. Wireless Conf.*, May 2016, pp. 1–6.

[6] R. Naderpour *et al.*, "Spatio-temporal channel sounding in a street canyon at 15, 28 and 60 GHz," in *Proc. 20th Int. Symp. Personal Indoor Mobile Radio Commun. (PIMRC'16)*, Valencia, Spain, Sep. 2016, pp. 1–5.

[7] J. Vehmas *et al.*, "Millimeter-wave channel characterization at Helsinki airport in 15, 28, and 60 GHz bands," in *Proc. 84th Veh. Tech. Conf. (VTC'16)*, Montreal, Canada, Sep. 2016, pp. 1–5.

[8] K. Haneda *et al.*, "Estimating the omni-directional pathloss from directional channel sounding," in *Proc. 10th Eur. Conf. Antenna and Propag. (EuCAP'16)*, Davos, Switzerland, Apr. 2016.

[9] S. Nguyen *et al.*, "Dual-band multipath cluster analysis of small-cell backhaul channels in an urban street environment," in *Proc. IEEE Global Commun. Conf. (GLOBECOM'16)*, Washington, USA, Dec. 2016.

[10] Wei. Fan *et al.*, "Comparative study of centimetric and millimetric propagation channels in indoor environments," in *10th Eur. Conf. Antennas and Propag. (EuCAP'16)*, Davos, Switzerland, Apr. 2016, pp. 1–5.

[11] I. Rodriguez *et al.*, "An empirical outdoor-to-indoor path loss model from below 6 GHz to cm-wave frequency bands," *IEEE Antennas and Wireless Propagation Letters (APWL)*, in press.

[12] O. H. Koymen *et al.*, "Indoor mm-wave channel measurements: Comparative study of 2.9 GHz and 29 GHz," in *Proc. IEEE Global Commun. Conf. (GLOBECOM'15)*, Dec. 2015, pp. 1–6.

[13] R. Muller *et al.*, "Simultaneous multi-band channel sounding at mm-wave frequencies," in *Proc. 10th Eur. Conf. on Antennas and Propag. (EuCAP'16)*, Davos, Switzerland, Apr. 2016, pp. 1–5.

[14] R. J. Weiler *et al.*, "Simultaneous millimeter-wave multi-band channel sounding in an urban access scenario," in *Proc. 9th Eur. Conf. on Antennas and Propag. (EuCAP'15)*, May 2015, pp. 1–5.

[15] S. Wyne *et al.*, "Beamforming effects on measured mm-wave channel characteristics," in *IEEE Trans. on Wireless Commun.*, vol. 10, no. 11, pp. 3553–3559, Nov- 2011.